Efficient Calculation of Large Finite Periodic Structures Based on Surface Wave Analysis

Xiaoyan Y.Z. Xiong, *Student Member, IEEE*, Ling Ling Meng, *Student Member, IEEE*, Li Jun Jiang, *Senior Member, IEEE*, Wei E.I. Sha, *Member, IEEE*, and Fan Yang, *Senior Member, IEEE*

***Abstract*—The electromagnetic modeling of practical finite periodic structures is a topic of growing interest. Due to the truncation of infinite periodic structures, surface waves will be excited and localized near discontinuous interfaces leading to the edge effect. In this work, surface waves are numerically extracted and their magnitudes and decay rates are analyzed for different materials and geometries. Based on the exponential decay of the surface wave, a novel method is developed by connecting the solution to the large finite array problem with that to a relatively small one to achieve low complexity and memory consumption. The method numerically reconstructs propagating Bloch waves and surface waves according to the Bloch-Floquet theorem of periodic structures and translation invariant properties of semi-infinite periodic structures, respectively. Numerical examples are shown for near-field distributions and far-field radiation patterns. The results obtained from small finite periodic structures capture the edge effect and agree well with the results by the rigorous element-by-element approach.**

***Index Terms*—Edge effect, finite periodic structures, frequency selective surface, leaky wave antenna, surface and Bloch waves.**

I. Introduction

PERIODIC structures have attracted a lot of attention in the past decades due to numerous applications such as metamaterials, antenna arrays, frequency selective surfaces (FSSs), photonic band gap (PBG) or electromagnetic band gap (EBG) structures, etc. [1]–[4]. Infinite periodic structures are impossible in a realistic fabrication. When truncating infinite periodic structures, discontinuities occur at truncation boundaries and surface waves will be excited according to the mode conversion, i.e., a mode incident to the discontinuity will excite many different modes [5]. Only allowed Bloch waves can propagate within the periodic structure. Surface waves become evanescent and localized around the discontinuities, which leads to the edge effect of finite periodic structures (FPSs). The prediction of wave natures in the edge elements of finite periodic structures is an indispensable procedure during the design of FPSs [6]–[8]. The element-by-element method and the infinite periodic approximation method are two conventional techniques used for FPSs. The former one is rigorous and captures all interactions between elements. It is suitable for small FPSs, but becomes computationally prohibitive for very large arrays. The latter one approximates the finite periodic structure as an infinite one so that the problem is reduced to the analysis of a single unit cell of the infinite periodic structure [9]. This technique yields good results for elements around the center of large arrays. However, it fails in predicting the wave behavior of elements close to edges or corners of the array. Hence, it is not sufficiently accurate for some engineering applications.

Several methods have been proposed to overcome problems in simulating large finite periodic structures. The first category bypassed difficulties by improving the computational capability of the existing methods. Among them, the fast multipole method [10], [11] and the domain decomposition method [12] are very powerful for modeling large FPSs.

Other methods consider edge effects with the help of an infinite periodic structure. In [13], the truncated Floquet wave method is used to solve a fringe integral equation in which the unknown function is the difference between the actual finite array and that of the associated infinite array. Although the solution of the infinite array problem needs to be determined first, the procedure to get the unknowns of the fringe integral equation is efficient since they can be simply and efficiently represented in terms of diffracted rays associated with truncated Floquet waves. Alternative methods are based on the convolution of the infinite array solution with an appropriate window function. The idea was first introduced in [14]. It is employed to compute the active input impedance of finite phased arrays of dipoles over a ground plane by the convolution implementation. Then, this method is extended to focus on the field rather than circuit quantities for phased arrays of microstrip patches [15]. Based on the Poisson's sum formula for finite sums, the electric field Green's function corresponding to a finite array becomes the product of the infinite array Green's function and the Fourier transform of the window function which defines the size of the finite array. Other methods proposed also belong to the windowing technique [16], [17].

Recently, entire-domain basis functions have been developed, i.e., macro basis function (MBF) [18] and synthetic basis function (SBF) [19], to analyze large array problems. Both MBF and SBF must capture the mutual coupling effect in an iterative process, which is time consuming. The characteristic basis function (CBF) is another entire-domain basis method

Manuscript received April 03, 2014; revised June 27, 2014; accepted October 10, 2014. Date of publication October 28, 2014; date of current version December 31, 2014. This work was supported in part by the Research Grants Council of Hong Kong (GRF 713011, 712612, and 711511), NSFC 61271158, US AF AOARD 124082 and 134140 contracted through UTAR, Hong Kong UGC AoE/P-04/08, and partially funded by Tsinghua National Laboratory for Information Science and Technology (TNList).

X. Y.Z. Xiong, L. L. Meng, L. J. Jiang, and W. E.I. Sha are with the Department of Electrical and Electronic Engineering, University of Hong Kong, Hong Kong, China (e-mail: xyxiong@eee.hku.hk).

F. Yang is with the Department of Electronic Engineering, Tsinghua University, Beijing 100084, China.

Color versions of one or more of the figures in this paper are available online at http://ieeexplore.ieee.org.

Digital Object Identifier 10.1109/TAP.2014.2365211

[20]. CBF includes the mutual coupling effect directly using a new type of high-level (secondary) basis function. In [21], [22], a new sub-entire-domain (SED) basis function method is utilized to analyze the scattering of patch arrays. The new basis function is defined on the support of each single cell of the periodic structure. The mutual coupling effects are taken into account in each single basis function by using dummy cells.

In this work, we developed a new efficient method to accurately calculate the electromagnetic (EM) response of large FPSs based on the extraction of surface waves. The rest of this paper is organized as follows. In Section II, we present the basic definition and theory for Bloch waves and surface waves of FPSs. In Section III, the magnitude and decay rate of surface waves of a multi-layer grating structure with different materials and geometric sizes are studied in detail. Section IV describes the approach of extracting the infinite periodic Bloch wave (IPBW) from the near-field data of the small FPS. We can employ the IPBW of the small FPS to reconstruct the IPBW of the large FPS, and so does the surface wave of the large FPS. In Section V, three large finite periodic structures involving a leaky wave antenna, a patch array and a dipole antenna array are investigated by the newly developed method. The results are compared to those by the element-by-element simulation. Excellent agreements are obtained and the proposed method saves considerable computer resources.

II. Surface Waves in Finite Periodic Structures

Regarding the dispersion relation (band diagram) of infinite periodic structures, e.g., 2-dimensional (2D) periodic structures with a 2D periodicity or 3D systems with a 3D periodicity, Bloch modes forming allowed bands support the propagation of EM waves through the structure. Given a fixed frequency and ignoring material (ohmic) losses, the allowed and forbidden bands have real and complex eigenvalues (Bloch wavenumbers), respectively. Hence, eigenmodes corresponding to allowed and forbidden bands are, respectively, propagating and evanescent modes. The complex Bloch wavenumber gives evanescent modes that cannot exist in infinite (bulk) crystals but can be excited at truncation edges of a finite crystal as bounded solutions.

There are two possible reasons for forming the surface wave in the finite periodic structure: (1) When the frequency of incident waves or excitation sources falls into the band gap, no propagating Bloch mode is allowed. Surface waves can be represented as a superposition of eigenmodes (evanescent modes) at the band gap frequency with complex Bloch wavenumbers. (2) When the frequency falls into the allowed band, both Bloch waves and surface waves can be excited simultaneously because of the momentum (phase) matching issue between the excitation source and Bloch wavenumber. Taking a dipole excitation and 2D finite periodic system (with the periodicity along one direction and truncation edges at the other direction) as an example, the dipole source generates plane waves (including evanescent waves) propagating toward various directions with distinguished wavenumbers k_x. Some wavenumbers of the plane waves can exactly or quasi-exactly match the allowed (propagating) Bloch wavenumber k_B, i.e., $k_x + 2\pi m/P = k_B$ or $k_x + 2\pi m/P = \Re(k_B)$, where $m = 0, \pm 1, \pm 2, \ldots$ and P is the periodicity in the x direction. For this situation, the Bloch wave is excited. Plane waves corresponding to mismatched wavenumbers will convert to surface waves according to the mode conversion. These surface waves, which can be represented as a superposition of eigenmodes at forbidden bands, decay exponentially on average toward the center of the periodic structure [23].

Regarding infinite periodic structures, e.g., 2D systems with the 1D periodicity or 3D systems with the 2D/1D periodicity, the guided wave, as a kind of propagating Bloch mode, has a nonzero imaginary part of the Bloch wavenumber along the periodicity direction due to the radiation (leaky) loss. Furthermore, surface waves also have a nonzero imaginary part of the propagation constant along the periodicity due to the truncation. However, surface waves and guided waves are distinguished physically. They can be well separated numerically because they have very different decay rates (attenuation constants). Surface waves decay much faster than guided waves even in a lossy plasmonic system [24]. In the eigenvalue analysis, we could identify the fundamental (propagating) Bloch modes by finding the minimum imaginary part of the Bloch wavenumber [25]. The truncation induced surface waves can be represented by the superposition of eigenmodes with large imaginary parts in their wavenumbers. We have investigated various periodic structures. The universally fast decay properties of surface waves are strongly verified. The separation of surface waves and guided waves is very feasible not only from physical but also from numerical aspects (please see following numerical results for leaky wave antennas). We will show the universally fast decay feature of surface waves in the next section.

III. Surface Wave Extraction and Analysis

This section numerically extracts surface waves. It demonstrates that they decay rapidly and will converge as the array size increases. These two important properties of surface waves of FPSs are analyzed by using the rigorous coupled-wave analysis (RCWA) method [26]. To simplify the analysis without losing generality, we investigate a 2D multi-layer grating structure in the xoz plane. It is periodic in the x direction with a periodicity of p_x. It is truncated in the z direction and bounded by Region I and Region III with the refractive indices of n_I and n_{III} (as shown in Fig. 1). n and N are the layer index and the total number of layers, respectively. d_n is the thickness of the nth layer. N_c denotes the index of the center layer. w_n is the width of the region occupied by the material with a relative permittivity of ε_r. To model finite periodic features in the z direction, each layer is forced to have the same thickness of $d_n = p_z$, the same material occupied width of $w_n = w$ and the same filling fraction of $f_n = w/p_x$. Each layer can be regarded as the cell of the periodic structure. Since the numerical convergence rate of RCWA at the TM polarization is much slower than that at the TE one [26] as shown in Fig. 2(c). Moreover regarding the 2D grating structure comprising materials with the single negative permittivity and excited by a plane wave, surface plasmon polariton-like (SPP-like) waves, which contribute significantly to surface waves, can only be excited by TM polarized plane waves. Hence, we only focus on the TM polarization case to understand and demonstrate the

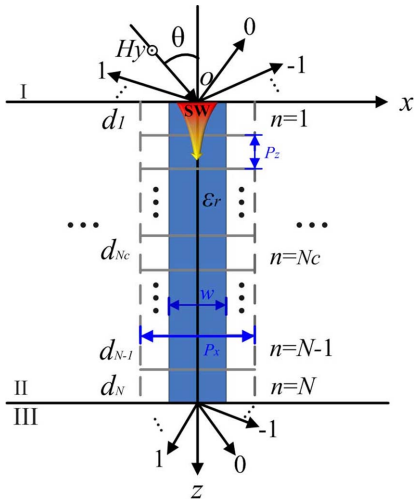

Fig. 1. Geometry of the multi-layer grating structure.

universal decay properties of surface waves. The multi-layer grating structure is illuminated by a normalized TM field of the form $H_{inc,y} = \exp\{-jk_0 n_I[\sin(\theta)x + \cos(\theta)z]\}$, where k_0 is the wavenumber in free space and θ is the incident angle. The fields in each cell and in Regions I and III can be calculated by the RCWA method.

The RCWA method is a generalized mode matching method that is very useful for modeling multi-layer periodic structures. It expresses the field of each cell in terms of space harmonics. Then the continuity boundary conditions for tangential EM fields are applied to determine expansion coefficients of each cell as well as reflection and transmission coefficients. Detailed descriptions of the RCWA theory are presented in [26], [27].

A. Surface Wave Extraction

For a sufficiently large number N, it is reasonable to assume that the center cell only contains infinite-periodic Bloch waves (IPBWs). However, due to the truncation, surface waves are excited and localized near the discontinuous boundaries at $z = 0$ and $z = Np_z$ planes. Hence, the total field is the superposition of surface waves and IPBWs. The infinite periodic approximation method ignores the contribution of surface waves, which leads to inaccurate results. When the magnitudes of surface waves are large or their decay rates are relatively slow, the surface wave effects are important and cannot be ignored. Hence, the magnitude and decay rate of surface waves can be adopted to evaluate the approximation error of the infinite periodic approximation method.

According to the above analysis, the total field is the superposition of surface waves and IPBWs. In other words, surface waves are differences between total fields and IPBWs. Therefore, the procedure for extracting surface waves is summarized as follows:

1) Calculate the total field of the structure with sufficiently large N through proper full wave electromagnetic solvers.
2) Get the IPBWs of the central cells that are similar to those in infinite periodic structures. Generally, this needs to solve an eigenvalue problem of a single cell with the periodic boundary condition (PBC). In our method, to avoid rigorously solving the eigenvalue problem, we extract IPBWs from the near field data of central cells as presented in Section IV-C.
3) Obtain surface waves by subtracting IPBWs from the total field.

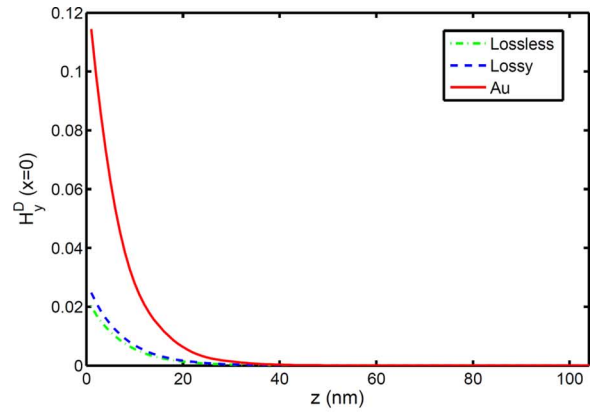

(a)

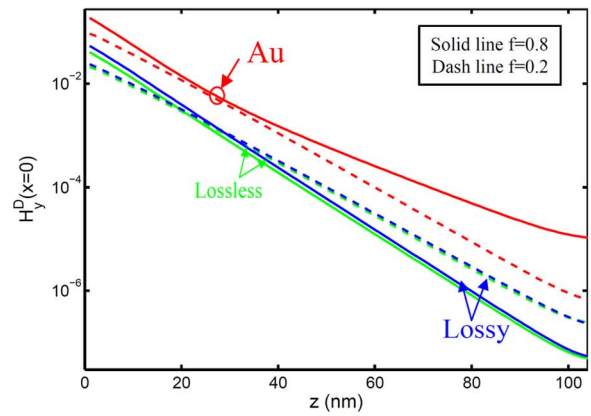

(b)

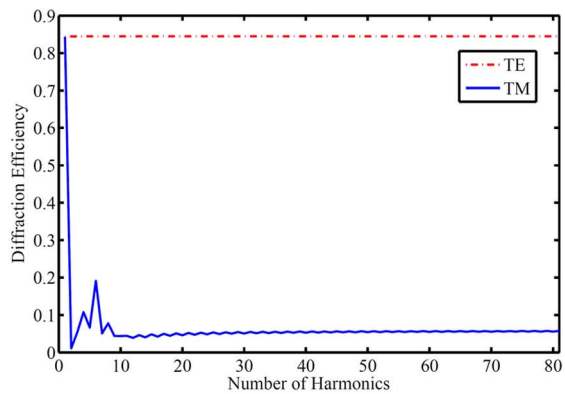

(c)

Fig. 2. Analysis of surface waves of the multi-layer grating structure (as shown in Fig. 1) for different materials and geometries. Parameters of the structure and computational setup: $\lambda = 620$ nm, $p_z = 10$ nm, $N = 21$, $p_x = 100$ nm, $\theta = 0°$, and $n_I = n_{III} = 1$ (air). TM (H_y) polarization. The permittivities of the lossless dielectric, lossy dielectric and lossy metal (Au) are $\varepsilon_r = 4$, $\varepsilon_r = 4 - j2$ and $\varepsilon_r = -10 - j2$ respectively. (a) filling factor $f = 0.5$; (b) filling factor $f = 0.2$ and $f = 0.8$ (logarithmic scale); (c) convergence behavior for simulation of the structure with lossy metal.

For the multi-layer grating structure with a large N, IPBWs of center cells are directly provided by the RCWA method since an eigenvalue problem has been solved in each cell to expand the field. IPBWs of center cells are defined as $\mathbf{F}^B(n = N_c)$, where "N_c" denotes the index of the center cell and "B" denotes the IPBW. IPBWs for other cells $\mathbf{F}^B(n)$ can be obtained by propagating $\mathbf{F}^B(N_c)$ along forward and backward directions based on obtained Bloch wavenumbers according to the Bloch-Floquet theorem. After getting the IPBWs $\mathbf{F}^B$ of the finite periodic structure, surface waves can be calculated by subtracting $\mathbf{F}^B$ from the total field $\mathbf{F}^{tot}$.

B. Surface Wave Analysis

Fig. 2(a) shows surface waves extracted by the proposed procedure for the multi-layer grating structure (see Fig. 1 for the configuration) with lossless dielectric, lossy dielectric and lossy metallic (single negative) materials. They decay rapidly for all cases. The amplitudes of surface waves in the dielectric structure are much smaller than those in the metal (Au) structure. This is expected because strong SPP-like waves [28] can be excited in periodic metallic structures that contribute significantly to surface waves. Fig. 2(b) presents the magnitude and decay rate of surface waves for different materials and different geometric dimensions ($f = 0.2$ and $f = 0.8$) as a function of the depth z in a logarithmic scale. Exponential decay trends are observed for all cases. Interestingly, the decay rates of surface waves are almost independent of the material types but closely related to geometries (periodicity, filling fraction, etc). This in fact agrees with theoretical results of [24], [29] where decay rates of surface waves are mainly governed by geometrical factors.

We note that the simulation for the lossy metal (single negative permittivity) structure has the serious numerical convergence problem. More space harmonics are needed to obtain accurate results. Fig. 2(c) displays the convergence of the diffraction efficiency [26] of the lossy metal case with the increasing number of space harmonics. 81 space harmonics are used for the lossy metal case. For the other two dielectric cases, 31 space harmonics are applied.

The cell number N is an important parameter to guarantee the accurate extraction of surface waves. Let us consider an extreme case by setting $N = 3$. Due to interferences between surface waves from two truncation edges, the field in the second cell ($N_c = 2$) is not of pure IPBWs. When we numerically propagate the EM field (spurious IPBWs) in the second cell forward and backward to the third and first cells, surface waves also travel forward and backward. When subtracting the spurious IPBW $\mathbf{F}^{B'}$ from the total field, the difference $\mathbf{F}^D = \mathbf{F}^{tot} - \mathbf{F}^{B'}$ is not the real surface wave we expected.

The convergence behavior of surface waves with respect to N is also studied by the RCWA method. First, surface waves of the structure with different N are extracted following the procedure presented in Section III-A. Second, after obtaining the surface wave, we monitor its magnitude with different N. As presented in Fig. 2, surface waves decay rapidly in the z direction. The maximum value of surface waves is located at the $z = 0$ interface. Hence, we define the maximum magnitude of surface waves as the average value along the x axis at the $z = 0$ interface as $H_y^M = 1/p_x \int_0^{p_x} H_y^D\big|_{z=0} dx$. Fig. 3 shows the maximum magnitude of surface waves with respect to the cell number N. It converges to a certain value when $N > 21$. Physically this can be explained by the translation invariant properties of semi-infinite periodic structures. Once the element number is sufficiently large, when we observe the structure from one side, e.g., the top side, the structure can be regarded as an infinite one extending to the other direction (i.e., the z-direction in Fig. 1). Increasing the number of layers will not change surface waves, which have gotten converged. Mathematically, the RCWA method expresses the field in each layer as the product of Bloch amplitude functions and exponential phase terms. The expansion coefficients are determined by matching boundary conditions at each layer interfaces. If the number of layers is large enough, the layers in the central region have the same expansion coefficients. When determining expansion coefficients corresponding to the top edge layers by matching boundary conditions, increasing the element number will not change those coefficients. In other words, the total field in the top edge layers will not be changed when the layer number N increases. This feature also holds true for surface waves since they are the subtraction of IPBWs from the total field. It means that the surface wave is converged. In other words, 21 cells are large enough to guarantee surface waves to die out at the center cell (the 11th layer). Hence, the center cell can be regarded as a unit cell in an infinite periodic array. Further increasing the number of cells will not change the magnitude of surface waves. An important conclusion can be drawn is that edge effects are invariant with respect to the increasing array size when N is sufficiently large for capturing the information of surface waves.

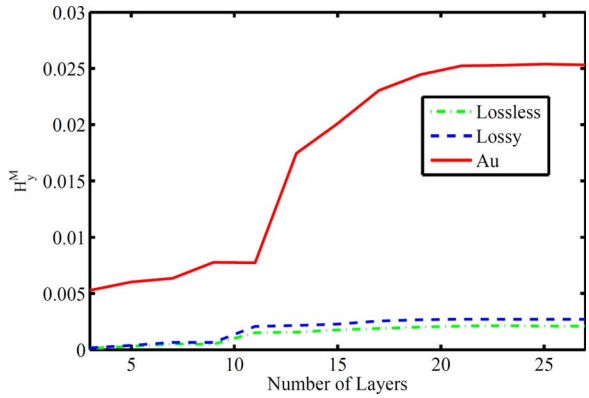

Fig. 3. Convergence of surface waves with the increasing cell number N for the 2D multi-layer grating structure (as shown in Fig. 1). $\lambda = 620$ nm, $p_z = 10$ nm, $p_x = 100$ nm, $\theta = 0°$, $f = 0.5$, $\varepsilon_{lossless} = 4$, $\varepsilon_{lossy} = 4 - j2$, $\varepsilon_{Au} = -10 - j2$, and $n_I = n_{III} = 1$ (air). TM (H_y) polarization.

We also check the dispersion relation of the center cell and compare it with the Bloch wavenumber of an infinite periodic structure. The MIT Photonic-Bands (MPB) software package [30] is used for the calculation. Here only the lossless case is considered because MPB can only handle lossless materials. As displayed in Fig. 4, when the frequency is not high, only one dominant (fundamental) mode exists in the center cell. Wavevectors of the center cell calculated by the RCWA method agree well with those of an infinite unit cell. This further confirms that the center cell only contains IPBWs.

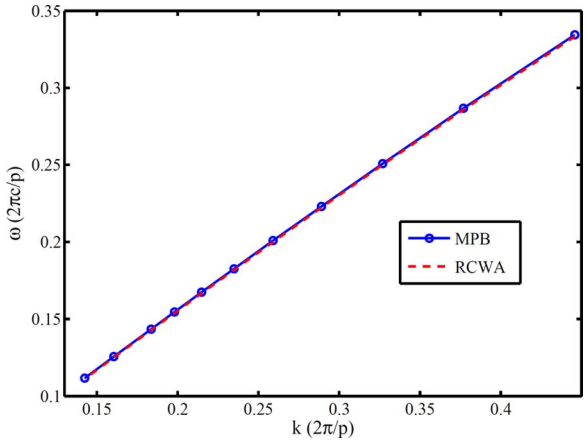

Fig. 4. Dispersion curve of the center cell calculated by the RCWA method and compared to that of the infinite periodic structure calculated by MPB. $\lambda = 620$ nm, $p_z = 10$ nm, $N = 21$, $p_x = 100$ nm, $\theta = 0°$, $f = 0.5$, $\varepsilon_r = 4$, $n_I = n_{III} = 1$ (air). TM (H_y) polarization.

IV. Field Reconstruction Process in Large Finite Periodic Structures

Inspired by the universal decay feature of surface waves and the conclusion that surface waves are invariant with respect to the increasing array size when the array is large enough, an efficient method is proposed to calculate large FPSs with fewer cells involved in the simulation. The procedure for 1D and 2D periodic structures is given below.

A. 1D Reconstruction Process

We begin with finite periodic structures with 1D periodicity. As shown in Fig. 5(a), the center unit cell of the large finite periodic structure is aligned with that of the small one. The cell number of the small finite periodic structure should be large enough to guarantee invariant (converged) surface waves. The field of the middle unit cell can be represented as the superposition of eigenmodes. These modes depend on factors such as periodicity, frequency, the structure feature, and so on. This kind of information is maintained by setting the small structure identical to the original large one except with fewer periodic cells. Given that the element number of the small finite structure is sufficiently large, the modes of the middle unit cell can be regarded as the same as those of the unit cell of an infinite one. Generally, only a few modes are important in expanding the field, leading to a reduced modal approximation [32], [33]. Hence, we can use the eigenmode expansion method to extract critical eigenmodes. Due to the termination of the structure, reflections at edges could propagate back into the finite periodic structure and change the internal field. These reflection-induced modes could be significant and need to be included during the IPBW extraction process. When the reflection is strong, numerous eigenmodes will be required to expand the field accurately. The cells of the small structure are classified into two regions: the IPBW region and the surface wave region. Central cells in the IPBW region only contain IPBWs and no surface wave exists in this region. Edge cells located at the two truncated sides belong to the surface wave region where both IPBWs and surface waves exist.

First, we simulate the small structure using proper full-wave solvers. They can be commercial software or in-house developed algorithms. Field distributions or equivalent sources are needed as simulation results.

Secondly, the IPBWs of the small structure in the IPBW region $\mathbf{F}^{B,S}$ are extracted by the eigenmode expansion method based on the near field data, e.g., for the center cell:

$$\mathbf{F}^{B,S}(x) = \sum_{m=1}^{M} \mathbf{\Psi}_m^S(x) \exp(-jk_{Bx,m}x), x \in \text{the } N_c \text{ cell} \tag{1}$$

where the superscript "S" denotes the small structure. $\mathbf{F}^{B,S}$ can be EM fields or equivalent sources. $\mathbf{\Psi}_m^S$ is the mth periodic Bloch-wave envelope function: $\mathbf{\Psi}_m^S(x) = \mathbf{\Psi}_m^S(x+P)$, with P as the periodicity in the x direction. $k_{Bx,m}$ is the mth IPBW wavenumber and can be complex due to the radiation or intrinsic (ohmic) loss. M is the number of modes used to expand the field in the IPBW region. Sec.

Thirdly, The IPBW obtained in the previous step is numerically propagated forward and backward to get IPBW of the large structure based on the Bloch-Floquet theory. The IPBW in both large and small structures are the same.

$$\begin{aligned}\mathbf{F}^{B,L}(x \pm \ell P) &= \mathbf{F}^{B,S}(x \pm \ell P) \\ &= \sum_{m=1}^{M} \mathbf{\Psi}_m^S(x) \exp\left(-jk_{Bx,m}(x \pm \ell P)\right) \\ &\quad x \in \text{ the cell } N_c\end{aligned} \tag{2}$$

where the superscript "L" denotes the large structure. ℓ is an integer.

Finally, EM fields or equivalent sources of the large structure in the surface wave region are reconstructed by using the translation invariant property of semi-infinite periodic structures. With respect to the left (right) surface wave region, the right (left) IPBW region can be approximated by semi-infinite periodic structures due to the fast decay of surface waves. Hence, the relationship between cells in the surface wave region and cells in the IPBW region (e.g., the relationship between cells $n = 1$ and $n = 3$) in the large structure shall be the same in the small structure. For cells belong to the surface waves region, we have

$$\frac{\mathbf{F}^{SW,L}(x)}{\mathbf{F}^{B,L}(N_{sw}+1)} = \frac{\mathbf{F}^{SW,S}(x)}{\mathbf{F}^{B,S}(N_{sw}+1)} \quad x \in \text{the surface waves region} \tag{3}$$

where $\mathbf{F}^{SW,L}$ and $\mathbf{F}^{SW,S}$ are fields in the surface wave region for large and small structures, respectively. $\mathbf{F}^{B,L}$ and $\mathbf{F}^{B,S}$ are fields in the IPBW region for large and small structures, respectively. N_{sw} is the number of cells in the surface wave region. For example, as shown in Fig. 5(a), $N_{sw} = 2$, according to (3), the relationship between the cells in the surface wave region and the IPBW region of the large structure shall be the same as the small one, e.g., $\mathbf{F}^{SW,L}(1)/\mathbf{F}^{B,L}(3) = \mathbf{F}^{SW,S}(1)/\mathbf{F}^{B,S}(3)$. Due to the propagation of IPBWs, both magnitude and phase adjustments are required to maintain the translation invariant property.

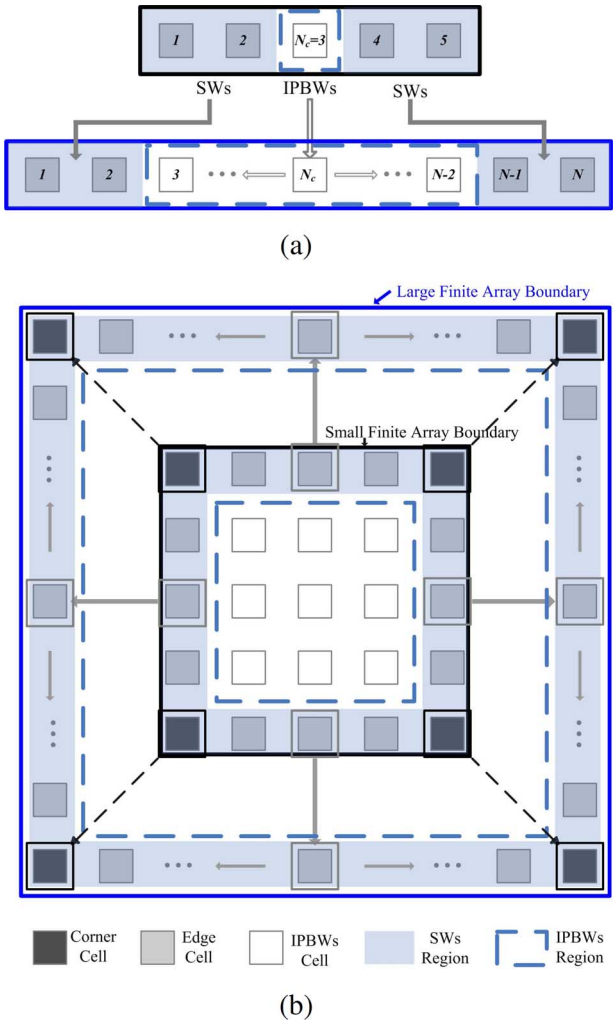

Fig. 5. Mechanism for the field reconstruction in large finite periodic structures from that of relative small ones. "SW" and "IPBW" are the short notations for surface wave and infinite-periodic Bloch wave, respectively. (a) Finite periodic structures with 1D periodicity. (b) Finite periodic structures with 2D periodicity.

B. 2D Reconstruction Process

Regarding the finite periodic structure with the 2D periodicity, the basic procedure to reconstruct the field of large structures is similar to the 1D case except that we now have corner cells in the surface wave region and IPBW wavenumbers in two directions, i.e., $k_{Bx,m}$ and $k_{By,m}$ along x and y directions, respectively. As shown in Fig. 5(b), corner cells and edge cells in the surface wave region of the small structure are used to reconstruct corner cells and edge cells of the large one. The center cell in the IPBW region of the small structure is used to reconstruct all cells in the IPBW region of the large structure. Note that phase and magnitude adjustments according to complex IPBW numbers are needed during the reconstruction process.

C. IPBW Extraction From the Near Field Data

To obtain Bloch waves of periodic structures rigorously, an eigenvalue problem needs to be solved. It is not trivial for complex structures with dispersive media. Some asymptotic methods have been developed to extract Bloch waves from FPS simulations. A commonly used one is the spatial Fourier transform (SFT) method. However, an accurate extraction can be obtained only for very large FPSs due to the fundamental limitation of the SFT method [31]. An alternative method extracts the dispersion relation of FPSs by considering the 1D FPS as a cascaded two-port network [34]. However the neglected surface wave effect leads to less accuracy. In this work, we extracted the Bloch waves of FPSs from the near field data of a few cells in the IPBWs region based on the eigenmode expansion. Let's consider a FPS with the x direction periodicity. M dominant modes are used in the frequency range of interest. The fields $\mathbf{F}(x,y,z)$ in the IPBW region can be expressed as a superposition of Bloch waves:

$$\mathbf{F}(x,y,z)=\underbrace{\sum_{m=1}^{M}\mathbf{\Psi}_m(x,y,z)\exp\left(-jk_{Bx,m}(x)\right)}_{\mathbf{F}^B(x,y,z)}+\mathbf{\Gamma}(x,y,z) \quad (4)$$

where $\mathbf{F}^B(x,y,z)$ includes the contribution from dominant modes. $\mathbf{\Gamma}$ is the difference between $\mathbf{F}(x,y,z)$ and $\mathbf{F}^B(x,y,z)$. It denotes the contribution from higher order modes with ignorable amplitudes. Then $\mathbf{\Psi}_m$ and $k_{Bx,m}$ can be retrieved using a standard minimization algorithm

$$\min_{\mathbf{\Psi}_m,k_{Bx,m}}\left\|\mathbf{F}(x,y,z)-\sum_{m=1}^{M}\mathbf{\Psi}_m(x,y,z)\exp(-jk_{Bx,m}(x))\right\|_2. \quad (5)$$

This is equivalent to finding the best fit to $\mathbf{\Psi}_m$ and $k_{Bx,m}$ by minimizing the maximum error between the near field data and the field reconstructed through dominant modes. The norm minimization is defined as the minimization of the maximum error.

For the numerical implementation, we can set the spatial sampling points for the finite periodic structure as $x=x_0+(n-1)P$, $y=const$, $z=const$, $n=1,2,\ldots,Q$, where Q is the cell number in the IPBW region and x_0 is located at the first cell in the IPBW region. Thus the spatial-dependent envelope function $\mathbf{\Psi}_m$ will become spatial-independent expansion coefficients a_m. The error distribution $\mathbf{\Gamma}$ of the objective function also provides a reference to judge the accuracy of extracted Bloch waves. If $\mathbf{\Gamma}$ is large, it means more IPBWs are needed in the extraction process. In addition, the sample point position x_0 can be randomly selected in the first unit cell of IPBWs. More series field data by varying the positions of x_0 can be used to improve the accuracy of the extraction procedure.

D. Limitations

To this end, the proposed method is based on the fast decay feature of surface waves. The IPBWs of large FPSs can be obtained from those of small FPSs according to the Bloch-Floquet theory. It requires that the electromagnetic fields produced by excited sources can be represented in terms of Bloch-Floquet modal functions. FPSs must have Bloch/Floquet sources, i.e., the cells shall be excited (or equivalently be excited) with uniform or linearly progressed amplitudes and phases.

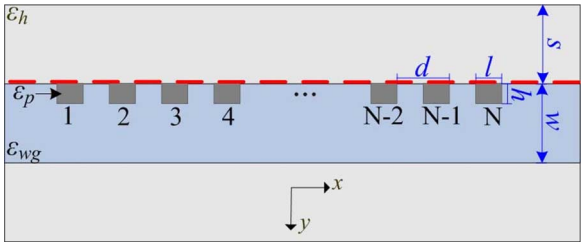

Fig. 6. LWA geometry. The dielectric waveguide is perturbed by the grating inside the waveguide. Refractive indices of the host medium, dielectric waveguide and perturbation cells are $n_h = 1.45$, $n_{wg} = 1.67$, $n_p = 3.48$. Other dimensions of the structure are: $d = 2\ell = 0.97$ um, $w = 1$ um, $h = 0.3$ um and $s = 20$ um. The perturbation cell number is $N = 60$. The dashed line represents the radiation aperture and the boundary where the field is extracted for far-field calculations.

V. Numerical Examples

A. Optical Leaky Wave Antenna

1) Leaky Wave Antenna by Periodic Structures: For a leaky wave antenna (LWA), the complex guided mode excited by the incoming field will leak power as it propagates along the antenna structure (x direction as in Fig. 6) [35]. Assume that the background medium is the same as the host medium with refractive index n_h, the wave in the background region above the antenna has the form of

$$\Psi(x, y) = \Psi_0 e^{-jk_x x} e^{+jk_y y} \tag{6}$$

where $k_x = \beta - j\alpha$ is the complex propagation constant. The wavenumber in the background media is $k_h = n_h k_0$. When $|\beta| < k_h$, the wave in the y direction can propagate and the structure can be used as an antenna. The radiation angle θ of the main beam of this antenna, defined from the normal direction (y), is then given by

$$\theta = \arcsin(\frac{\beta}{k_h}). \tag{7}$$

According to the antenna theory, high directivity requires a large radiation aperture. So the attenuation constant α shall be small to allow a long antenna aperture. As a result, a large number of periodic cells are needed. Here we analyze a classical LWA by a dielectric waveguide with small perturbations from grating cells (see Fig. 6). The geometric parameters are taken from [36], [37]. Here, we focus on the efficient calculation rather than the antenna design. The LWA is excited by the even dielectric waveguide mode at the left side with the electric field polarized in the z direction and traveling in the x direction with a free space wavelength $\lambda_0 = 1550$ nm. The simulation is conducted by an in-house developed finite-difference time-domain (FDTD) method [38]. All of the results in this manuscript were performed on an Intel Xeon 2.67 GHz processor. The unit of the FDTD cubic grid is $\delta s = 30.3125$ nm. The time step is $\delta t = \delta s/2c$, where c is the light speed in free space.

2) IPBW Extraction: The electric field along the periodic structure can be represented as the superposition of Bloch-Floquet space harmonics. The excited leaky mode in the practical design is usually the -1 space harmonic ($k_m = k_{wg} + 2\pi m/p_x, m = -1$) and others are suppressed. For the finite LWA, due to the truncation at the end side, a backward leaky wave also exists in the antenna. Since only the -1 space harmonic is relevant to the radiation, the field in the IPBW region of the antenna radiation aperture (the dashed line in Fig. 6) can be represented by two Bloch waves $(\mathrm{M} = 2)$ propagating forward and backward with wavenumbers $k^+ = k_{-1} = \beta_{-1} - j\alpha$ and $k^- = -k^+$ respectively.

$$E_z(x) = a^+ E_z^+(x) e^{-jk^+ x} + a^- E_z^-(x) e^{-jk^- x} \tag{8}$$

where $a^\pm$ and $E_z^\pm$ are the coefficients and the periodic Bloch-wave envelope functions of the forward and backward waves respectively. $E_z^\pm(x + p_x) = E_z^\pm(x)$ and p_x is the periodicity in the x direction.

Instead of calculating the original leaky wave antenna with $N = 60$, we calculate a relatively smaller one with $N = 30$. The middle 10 cells ($n = 11$ to $n = 20$) are considered as the IPBW region. From (8), to obtain IPBWs in middle cells, we need to extract two parameters β_{-1} and α from the field along the waveguide. We follow the proposed procedure in Section IV. The field is sampled at one point per cell $x_n = x_0 + np_x, n = 1, 2, \ldots, 10$ (the right corner of each perturbation cell along x direction). It has the form of $E_z(n) = a^+ E_z(11) e^{-jk^+ p_x(n-11)} + a^- E_z(11) e^{-jk^- p_x(n-11)}$. By employing the least mean square method, we get $k^+ = \beta - j\alpha = -2.48 \times 10^5 - j4.40 \times 10^4$, $a^+ = 1.097$ and $a^- = -0.097$.

After extracting IPBWs from the small LWA ($N = 30$), IPBWs of the center unit cell ($N_c = 15$) are propagated forward and backward to reconstruct IPBWs of the original large LWA ($N = 60$). This procedure is equivalent to terminating the LWA with matched Bloch impedance and modelling the LWA as an infinite periodic structure. Because surface wave effects are ignored, the constructed IPBWs are equivalent to those simulated by the infinite periodic approximation method. Fig. 7 shows the magnitude and phase of reconstructed IPBWs. They are compared to those from the element-by-element calculation. In the IPBW region they agree well with each other, which validates the accuracy of extracted IPBWs from the small LWA. However, discrepancies between the element-by-element calculation and reconstructed IPBWs in the surface wave regions clearly indicate the presence of surface waves. Hence, if the LWA is not terminated by the matched Bloch impedance, surface wave effects cannot be ignored and the infinite periodic approximation method is inaccurate to model the finite structure. The field represented by only one dominant forward leaky mode ($M = 1$) is also presented in Fig. 7. The magnitude of the field in Fig. 7(a) exhibits a major linear trend with a logarithmic scale, which confirms its exponential decay in the x direction. However, the reflected backward leaky wave is not captured if only one forward IPBW is extracted. The backward leaky wave is caused by the discontinuity at the end side of the antenna. The IPBWs inside the LWA are the superposition of both forward and backward leaky waves. Since the magnitude of the backward leaky wave is much smaller than the forward one, the magnitude of the total IPBW maintains the major exponentially decay trend as shown in Fig. 7(a). However, due to the co-existence of the backward leaky wave and the forward leaky

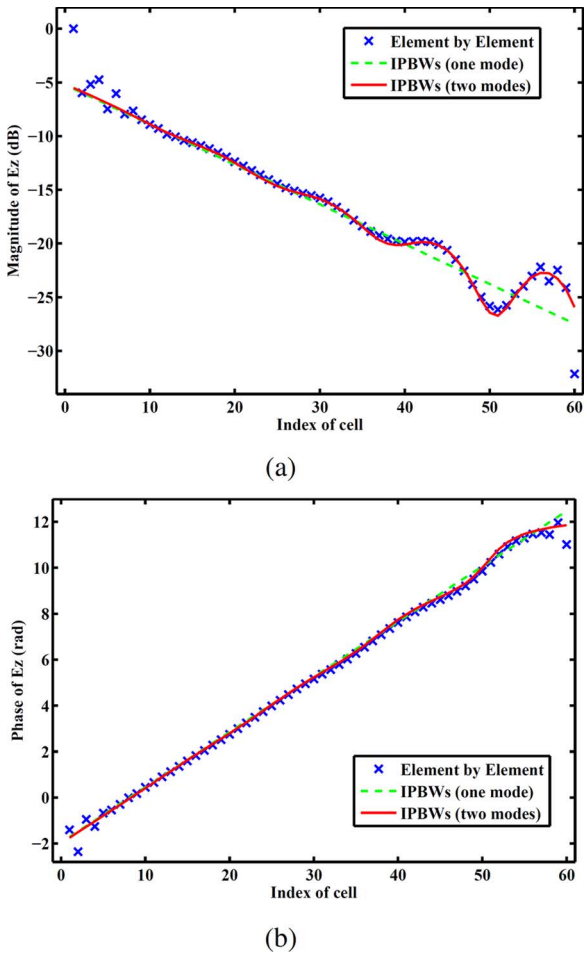

Fig. 7. Electric field along the radiation aperture, sampled in perturbation cells (one point per cell). (a) Magnitude. (b) Phase.

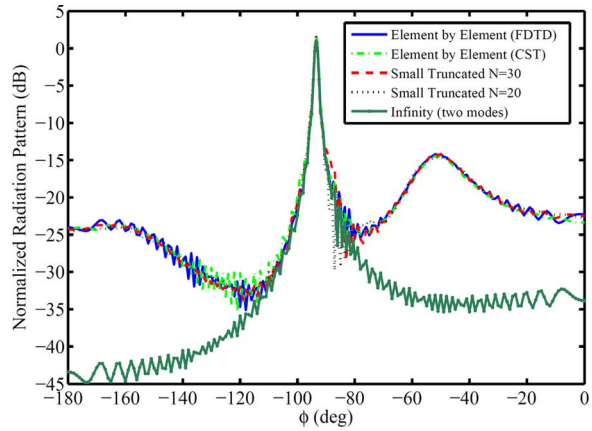

Fig. 8. Comparisons of the normalized far-field radiation patterns of the leaky wave antenna simulated by different methods. The solid and dash-dot lines are the element-by-element results of the $N = 60$ structure calculated by the in-house developed FDTD method and the commercial software CST. The dashed line and dotted line are the results calculated based on simulations for $N = 30$ and $N = 20$ structures, respectively. The marked solid line is the result of an infinite periodic array with $N = 60$.

wave, two leaky modes will form a cosine function (two exponential terms with opposite signs). Hence, the magnitude of total IPBWs containing two modes will have a weak standing wave pattern. In addition, compared with the rigorous element-by-element method, large discrepancies are observed if only one forward leaky wave is considered while better agreements are observed for the two-mode case. This indicates that the backward leaky wave is also important for accurately modeling the EM response of finite LWAs.

3) Near-Field Reconstruction and Far-Field Radiation Pattern: After getting IPBWs of the small structure with $N = 30$, the field of the original large structure with $N = 60$ can be reconstructed from the information of the $N = 30$ structure. First, the field of middle cells (i.e., $n = 21$ to $n = 50$) can be obtained by propagating IPBWs extracted from the small structure according to (2). The edge cells ($n = 1$ to $n = 10$ and $n = 51$ to $n = 60$) can be replaced by those of the small structure with proper phase and magnitude. After obtaining the near field of the radiation aperture, the far-field radiation pattern can be easily computed using the Stratton-Chu integral equation [39].

Fig. 8 shows that far-field radiation patterns obtained by the proposed method are in good agreement with element-by-element simulation results. We can see that the main beam located at around $\theta = -93.5°$ agrees well with the theoretical model from (6). The sidelobe around $-52°$ due to the presence of surface waves is not correctly predicted by the infinite periodic approximation method. Hence, for finite LWAs without matched terminations, surface wave effects are critical for predicting the sidelobes. However, in practice, it is difficult to know if the size of the small structure is large enough to capture the critical information of surface waves. In order to verify the accuracy of the result, we need to calculate another small structure with the different element cell number. If the results calculated by these two small structures do not agree with each other, we need to increase the size of the small structure further. The far-field radiation pattern from a small structure with $N = 20$ is also tested. 8 middle cells are considered as the IPBW region and 6 edge cells at each side form surface wave regions. Only small discrepancies are observed in Fig. 8. It means the $N = 30$ structure is large enough to capture all the surface wave information.

The computational cost of the proposed method includes two parts: one part is to simulate a small structure with fewer cells. The other one is to extract and reconstruct IPBWs. As for the first part, because the unknowns are proportional to the number of unit cells, modeling the small structure with fewer unit cells results in significant CPU time and memory savings, especially for 2D or 3D FPSs. As for the second part, due to the rapid decay feature of surface waves and limited propagating Bloch modes, usually several sample points in the IPBW region are enough to extract IPBWs accurately (e.g., only 10 sample points in the IPBW region of the small LWA are used). The computational cost for the second part can be ignored compared to the first part. Hence, the total computational cost of the proposed method is much less than that of the element-by-element simulation method.

Table I compares the computational information for the LWA with different perturbation cells. Obviously the proposed method can save CPU time and memory significantly. Furthermore, when the number of unit cells increases for large structures, we can reuse the information of surface waves and IPBWs provided by the same small structure to reconstruct

TABLE I
THE COMPUTATIONAL INFORMATION OF AN LWA WITH DIFFERENT PERTURBATION CELLS

Elements	N=20	N=30	N=60
Domain (μm^2)	32.37×43.97	42.07×43.97	71.17×43.97
Memory (MB)	47	62	104
Time steps (δt)	21440	27840	34240
CPU time (s)	381.65	782.47	1548.84/860(CST)

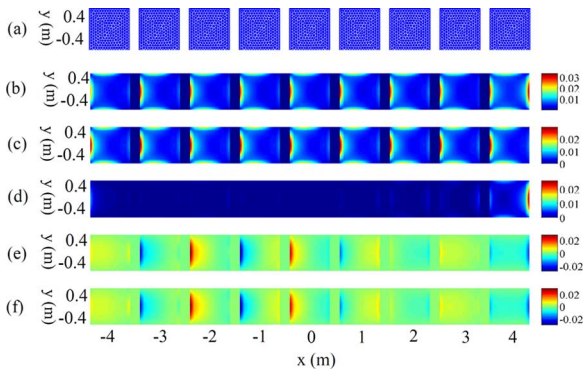

Fig. 9. (a) Geometry of a finite FSS array, truncated in the x direction; (b), (c) and (d) magnitude of original (element-by-element simulation with $N_x = 9$ patch cells), infinite (produced by the center unit cell) and surface wave currents, respectively; (e) imaginary parts of the currents of the original patch array (element-by-element simulation); (f) imaginary parts of the currents reconstructed by the $N_x = 5$ patch array.

relevant EM fields, which is very useful to predict the performance of large finite periodic structures.

B. Patch Array FSS

1) Patch Array With 1D Periodicity: The proposed method can be used to efficiently simulate a finite patch array FSS that has numerous applications in telecommunications. We first consider a finite array with 1D periodicity along the x direction. The geometry is shown in Fig. 9(a). Metallic patches with the size of $0.8\ \mathrm{m} \times 0.8\ \mathrm{m}$ are in the $x - y$ plane. Their periodicity is truncated in the x direction. The gap between adjacent patches is $0.2\ \mathrm{m}$. The periodicity along the x direction is $p_x = 1\ \mathrm{m}$. The array is illuminated by a plane wave with the incident angle $\theta = 45°$ and $\phi = 0°$. The incident frequency is 240 MHz. In the conventional method, this type of array was treated as an infinite structure and only a single cell of the periodic structure needs to be considered. However, the surface wave contribution cannot be ignored. Using the proposed method, we obtain the results of an array with $N_x \times N_y = 9 \times 1$ patches from a relatively small one with $N_x \times N_y = 5 \times 1$ patches. The induced surface current on each patch of the small array is computed by the method-of-moment (MOM) method [40], [41].

The same procedure is used to efficiently calculate the $N_x = 9$ (1D) patch array. First, the surface currents of a small array with $N_x = 5$ are extracted from the middle three cells ($n = 2$ to $n = 4$). Only one IPBW ($M = 1$) is extracted. The Bloch wavenumber extracted is $k_{Bx} = k_{x0}\sin(\theta) = 3.557\ \mathrm{rad/m}$. Then currents in the center cell of the small array are used to reconstruct currents in the middle cells of the large patch array ($n = 2$ to $n = 8$). The first and last cells of the large structure are simply replaced by the first and last cells of the small structure (with phase manipulations according to (3)). Figs. 9(b) and 9(c) show the magnitudes of currents on each patch by the element-by-element simulation and IPBW currents extracted from the $N_x = 5$ patch array, respectively. Fig. 9(d) shows the magnitude of surface wave currents obtained by subtracting IPBW currents from those calculated by the element-by-element method. Only the first and last patches show obviously different EM responses. It suggests that the surface wave decays fast and only affects the terminating patches of the array. To validate both magnitude and phase, Figs. 9(e) and 9(f) compare the imaginary parts of the currents calculated by the element-by-element method with those reconstructed from the small patch array ($N_x = 5$). They agree with each other very well.

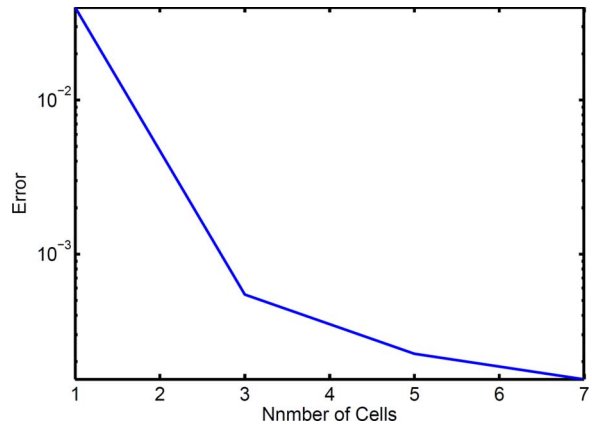

Fig. 10. The error between the element-by-element method and the proposed method as a function of the cell number N involved in the small 1D patch array.

The accuracy of the proposed method with respect to the cell number N in the small structure is investigated quantitatively. The error between the element-by-element method and the proposed method is defined as $\mathbf{J}^{err} = \left|\left|\mathbf{J}^{ebe} - \mathbf{J}^{re}\right|\right|_2$, where $\mathbf{J}^{ebe}$ and $\mathbf{J}^{re}$ are the equivalent surface current on patches calculated by the element-by-element method and the proposed method, respectively. Fig. 10 shows the error as a function of the cell number N. The error decreases with the increasing cell number. Eventually, the error disappears when the cell number involved in the small structure equals to that of the original large one. There is a trade-off between the efficiency and accuracy. Increasing the size of the small structure improves the accuracy but sacrifices the efficiency.

2) Patch Array With 2D Periodicity: We extend the developed method to calculate a finite patch array with 2D periodicity. A patch array with the same cell size ($0.8\ \mathrm{m} \times 0.8\ \mathrm{m}$) and periodicity along the x and y directions ($p_x = p_y = 1\ \mathrm{m}$) is illuminated by a plane wave ($f = 240\ \mathrm{MHz}$). The incident angle is set to $\theta = 45°$ and $\phi = 45°$. The currents of a large patch array with $N_x \times N_y = 9 \times 9$ cells are efficiently reconstructed from a small array with $N_x \times N_y = 5 \times 5$ cells by using the same procedure as described in Section IV with $k_{Bx} = k_{x0}\sin(\theta)\cos(\phi) = 2.513\ \mathrm{rad/m}$ and $k_{By} = k_{x0}\sin(\theta)\sin(\phi) = 2.513\ \mathrm{rad/m}$. Figs. 11(a) and 11(b) show the imaginary parts of the currents calculated by the element-by-element method 9×9 and by the proposed approach from the small patch array 5×5. Excellent agreements are observed.

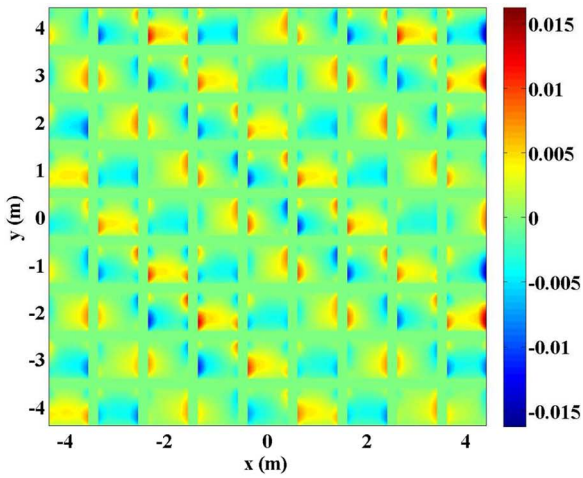

Fig. 11. Imaginary parts of the currents on the patch array. (a) original currents (element-by-element simulation with 9 ×9 cells). (b) reconstructed currents from the small 5 ×5 patch array.

After having the current reconstructed on the patches, the far-field pattern is calculated from the near-to-far-field transformation. Fig. 12 shows the radar cross section (RCS) calculated by different methods. Again, the results obtained from the small structure agree well with the element-by-element results while the infinite periodic array method fails in predicting sidelobes (around 10 dB deviations are observed at $\theta = 47°$ and $\theta = 133°$) due to the loss of the surface wave information.

Table II shows the computational information of the patch array FSS with different cell numbers simulated on the same computer. Again, the developed method is efficient for large finite periodic structures.

C. Dipole Antenna Array

The proposed method is also used to efficiently calculate a dipole antenna array (DAA) with $N_x \times N_y = 11 \times 11$ cells. The inset in Fig. 13 shows the configuration of a unit cell of the DAA. The total dipole length is $l = 0.39$ m and the dipole width is $w = 0.01$ m. The thickness of the substrate is $t = 0.19$ m. The substrate is air with relative permittivity $\varepsilon_r = 1$ on the ground plane. The size of the unit cell is $p_x \times p_y = 0.5$ m $\times$ 0.5 m. Each dipole is excited by the Delta-gap source with frequency $f = 300$ MHz. Again, instead of simulating the large DAA, we calculate two small antenna arrays with $N_x \times N_y = 3 \times 3$ and 5 $\times$ 5 cells to predict the behavior of the original DAA. The surface currents on dipole patches and the ground plane are computed by the method-of-moment (MoM) method. Fig. 13 shows the radiation patterns calculated based on different number of array cells. As we can see, there are small discrepancies between

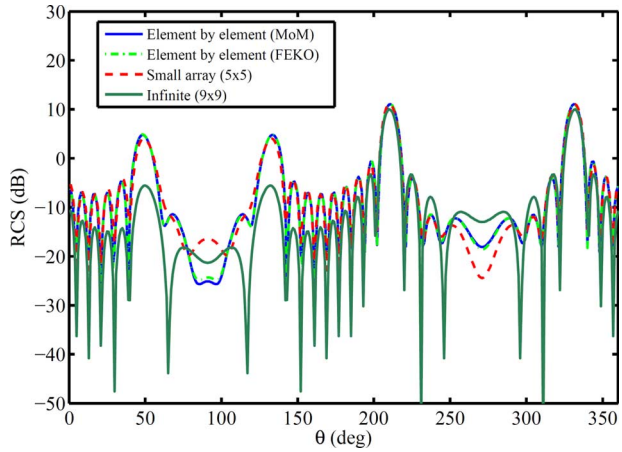

Fig. 12. Comparison of RCS calculated by different methods. The solid and dash-dot lines are, respectively, the element-by-element results of the original 9 × 9 patch array simulated by the MoM method and the commercial software FEKO; the dashed line is the result calculated from the small 5× 5 patch array; the marked solid line is the result from an infinite periodic patch array with 9 × 9 cells.

TABLE II
THE COMPUTATIONAL INFORMATION OF THE PATCH ARRAY FSS WITH DIFFERENT CELL NUMBERS

Elements ($N_x \times N_y$)	(5×1)	(9×1)	(5×5)	(9 × 9)
No. of RWG basis	1002	1852	5012	16665
Memory (MB)	15	52	383	4238
No. of iterations	27	39	106	267
CPU time (s)	12	43	116	926/771(FEKO)

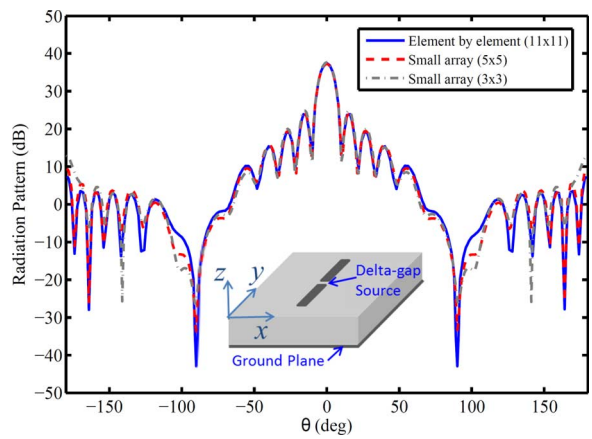

Fig. 13. Comparison of radiation patterns calculated by different methods. The solid line is the element-by-element result of the original 11 × 11 dipole antenna array simulated by the MoM method; the dashed and the dash-dot lines are the results calculated from the small 5 × 5 and 3 × 3 dipole antenna arrays, respectively. The inset shows the configuration of a unit cell of the dipole antenna array. The total dipole length is 0.39 m and the dipole width is 0.01 m. The thickness of the substrate is 0.19 m. The size of the unit cell is $p_x \times p_y = 0.5$ m $\times$ 0.5 m. The substrate is air with $\epsilon_r = 1$ on the ground plane.

TABLE III
THE COMPUTATIONAL INFORMATION OF THE DIPOLE ANTENNA ARRAY WITH DIFFERENT CELL NUMBERS

Elements ($N_x \times N_y$)	(3×3)	(5×5)	(11×11)
No. of RWG basis	2041	6122	19849
Memory (MB)	63	571	6012
No. of iterations	47	132	311
CPU time (s)	62	172	1610

the results calculated based on the 3×3 array and those based on the original 11×11 array. When we increase the size of the small array to 5×5, the accuracy is improved and the results agree better with the rigorous element-by-element method. For antenna designs, it is reasonable to begin with a small structure with 5×5 elements (or 5 elements for structures with 1D periodicity). Then we can check the field distribution of central elements. Large discrepancies mean the mutual couplings between elements are strong and surface waves decay slowly. If this is the case, one needs to increase the size of the small structure. Table III shows the computational information of the DAA with different cell number. The proposed method is fairly efficient for simulating large finite periodic structures compared to the element-by-element method.

VI. CONCLUSION

This paper provides the theoretical background and the numerical method for the surface waves extraction and their effects on finite period structures. The magnitude and decay rate of surface waves regarding to different materials and geometric sizes are calculated and analyzed. Based on the rapid decay property of surface waves, an efficient method for modeling large finite periodic structures is developed. From a small finite periodic structure that contains all the information of surface waves and IPBWs, we can accurately predict the performance of large finite periodic structures without ignoring the edge effect. Numerical examples are used to validate the accuracy and efficiency of the method. The observed edge effect strongly affects sidelobes of arrays and should not be ignored.

REFERENCES

[1] C. M. Soukoulis and M. Wegener, "Past achievements and future challenges in the development of three-dimensional photonic metamaterials," *Nat. Photon.*, vol. 5, pp. 523–530, Sep. 2011.

[2] V. M. Shalaev, "Optical negative-index metamaterials," *Nat. Photon.*, vol. 1, pp. 41–48, Jan. 2007.

[3] B. A. Munk, *Frequency Selective Surfaces: Theory and Design*. New York, NY, USA: Wiley, 2000.

[4] G. Papanicolau, A. Bensoussan, and J. L. Lions, "Asymptotic analysis for periodic structures," *Amer. Math. Soc.*, 2011.

[5] R. E. Collin, *Field Theory of Guided Waves*. New York, NY, USA: McGraw-Hill, 1960.

[6] W. L. Ko and R. Mittra, "Scattering by a truncated periodic array," *IEEE Trans. Antennas Propag.*, vol. 36, pp. 496–503, Apr. 1988.

[7] B. Tomasic and A. Hessel, "Analysis of finite arrays—a new approach," *IEEE Trans. Antennas Propag.*, vol. 47, pp. 555–565, Mar. 1999.

[8] A. Cucini, M. Albani, and S. Maci, "Truncated Floquet wave full-wave ($T(FW)^2$) analysis of large periodic arrays of rectangular waveguides," *IEEE Trans. Antennas Propag.*, vol. 51, pp. 1373–1385, Jun. 2003.

[9] F. Capolino, D. R. Wilton, and W. A. Johnson, "Efficient computation of the 2-D Green's function for 1-D periodic structures using the Ewald method," *IEEE Trans. Antennas Propag.*, vol. 53, pp. 2977–2984, Sep. 2005.

[10] R. Coifman, V. Rokhlin, and S. Wandzura, "The fast multipole method for the wave equation: A pedestrian prescription," *IEEE Antennas Propag. Mag.*, vol. 35, pp. 7–12, 1993.

[11] W. C. Chew, J. M. Jin, E. Michielssen, and J. M. Song, *Fast and Efficient Algorithms in Computational Electromagnetics*. Norwood, MA, USA: Artech House, 2001.

[12] J. B. Manges, J. W. Silvestro, and K. Zhao, "Finite-element analysis of infinite and finite arrays," *Int. J. Microw. Wireless Technol.*, vol. 4, pp. 357–364, Jun. 2012.

[13] A. Neto, S. Maci, G. Vecchi, and M. Sabbadini, "A truncated Floquet wave diffraction method for the full wave analysis of large phased arrays. I. basic principles and 2-D cases," *IEEE Trans. Antennas Propag.*, vol. 48, pp. 594–600, Apr. 2000.

[14] A. Ishimaru, R. Coe, G. Miller, and P. Geren, "Finite periodic structure approach to large scanning array problems," *IEEE Trans. Antennas Propag.*, vol. 33, pp. 1213–1220, Nov. 1985.

[15] A. K. Skrivervik and J. R. Mosig, "Analysis of finite phase arrays of microstrip patches," *IEEE Trans. Antennas Propag.*, vol. 41, pp. 1105–1114, Aug. 1993.

[16] A. K. Skrivervik and J. R. Mosig, "Finite phased array of microstrip patch antennas: The infinite array approach," *IEEE Trans. Antennas Propag.*, vol. 40, pp. 579–582, May 1992.

[17] A. J. Roscoe and R. A. Perrott, "Large finite array analysis using infinite array data," *IEEE Trans. Antennas Propag.*, vol. 42, pp. 983–992, Jul. 1994.

[18] E. Suter and J. Mosig, "A subdomain multilevel approach for the MoM analysis of large planar antennas," *Microw. Opt. Technol. Lett.*, vol. 26, pp. 270–227, Aug. 2000.

[19] L. Matekovits, G. Vecchi, G. Dassano, and M. Orefice, "Synthetic function analysis of large printed structures: The solution space sampling approach," in *Proc. IEEE AP-S Int. Symp.*, Boston, MA, USA, Jul. 2001, pp. 568–571.

[20] J. Yeo, V. V. S. Prakash, and R. Mittra, "Efficient analysis of a class of microstrip antennas using the characteristic basis function method (CBFM)," *Microw. Opt. Technol. Lett.*, vol. 39, pp. 456–464, Dec. 2003.

[21] W. B. Lu, T. J. Cui, Z. G. Qian, X. X. Yin, and W. Hong, "Accurate analysis of large-scale periodic structures using an efficient sub-entire-domain basis function method," *IEEE Trans. Antennas Propag.*, vol. 52, pp. 3078–3085, Nov. 2004.

[22] W. B. Lu, T. J. Cui, X. X. Yin, Z. G. Qian, and W. Hong, "Fast algorithms for large-scale periodic structures using subentire domain basis functions," *IEEE Trans. Antennas Propag.*, vol. 53, pp. 1154–1162, Mar. 2005.

[23] A. P. Vinogradov, A. V. Dorofeenko, A. M. Merzlikin, and A. A. Lisyansky, "Surface states in photonic crystals," *Phys.-Uspekhi*, vol. 53, pp. 243–256, Mar. 2010.

[24] X. Y. Z. Xiong, L. J. Jiang, V. A. Markel, and I. Tsukerman, "Surface waves in three-dimensional electromagnetic composites and their effect on homogenization," *Opt. Expr.*, vol. 21, pp. 10412–10421, 2013.

[25] W. E. I. Sha, L. L. Meng, W. C. H. Choy, and W. C. Chew, "Observing abnormally large group velocity at the plasmonic band edge via a universal eigenvalue analysis," *Opt. Lett.*, vol. 39, no. 1, pp. 158–161, Jan. 2014.

[26] M. G. Moharam, E. B. Grann, D. A. Pommet, and T. K. Gaylord, "Formulation for stable and efficient implementation of the rigorous coupled-wave analysis of binary gratings," *J. Opt. Soc. Am. A*, vol. 12, pp. 1068–1076, May 1995.

[27] M. G. Moharam, D. A. Pommet, and E. B. Grann, "Stable implementation of the rigorous coupled-wave analysis for surface-relief gratings: enhanced transmittance matrix approach," *J. Opt. Soc. Am. A*, vol. 12, pp. 1077–1086, May 1995.

[28] H. Raether, *Surface Plasmons on Smooth and Rough Surfaces and on Gratings*. Berlin: Springer, 1988.

[29] V. A. Markel and J. C. Schotland, "Homogenization of maxwell's equations in periodic composites: Boundary effects and dispersion relations," *Phys. Rev. E*, vol. 85, p. 066603, 2012.

[30] S. G. Johnson and J. D. Joannopoulos, "Block-iterative frequency-domain methods for maxwell's equations in a planewave basis," *Opt. Expr.*, vol. 8, pp. 173–190, Jan. 2001.

[31] H. Gersen, T. J. Karle, R. J. P. Engelen, W. Bogaerts, J. P. Korterik, N. F. Hulst van, T. F. Krauss, and L. Kuipers, "Direct observation of Bloch harmonics and negative phase velocity in photonic crystal waveguides," *Phys. Rev. Lett.*, vol. 94, pp. 123901–4, 2005.

[32] Q. I. Dai, Y. H. Lo, W. C. Chew, Y. G. Liu, and L. J. Jiang, "Generalized modal expansion and reduced modal representation of 3-D electromagnetic fields," *IEEE Trans. Antennas Propag.*, vol. 58, pp. 3856–3864, Feb. 2014.

[33] Q. I. Dai, W. C. Chew, Y. H. Lo, Y. G. Liu, and L. J. Jiang, "Generalized modal expansion of electromagnetic field in 2-D bounded and unbounded media," *IEEE Antennas Wireless Propag. Lett.*, vol. 11, pp. 1052–1055, 2012.
[34] G. Valerio, S. Paulotto, P. Baccarelli, P. Burghignoli, and A. Galli, "Accurate Bloch analysis of 1-D periodic lines through the simulation of truncated structures," *IEEE Trans. Antennas Propag.*, vol. 59, pp. 2188–2195, Jun. 2011.
[35] F. Capolino, *Applications of Metamaterials*. Boca Raton, FL, USA: CRC Press, 2009.
[36] S. Campione, C. Guclu, Q. Song, O. Boyraz, and F. Capolino, "An optical leaky wave antenna with Si perturbations inside a resonator for enhanced optical control of the radiation," *Opt. Expr.*, vol. 20, pp. 21305–21317, Sep. 2012.
[37] Q. Song, S. Campione, O. Boyraz, and F. Capolino, "Silicon-based optical leaky wave antenna with narrow beam radiation," *Opt. Expr.*, vol. 19, pp. 8735–8749, Apr. 2011.
[38] X. Y. Z. Xiong and W. E. I. Sha, "The FDTD method: Essences, evolutions, and applications to nano-optics and quantum physics," in *Computational Nanotechnology Using Finite Difference Time Domain*. Boca Raton, FL, USA: CRC Press, 2013, pp. 37–82.
[39] E. J. Rothwell and M. J. Cloud, *Electromagnetics*. Boca Raton, FL, USA: CRC Press, 2009, p. 418.
[40] R. F. Harrington, *Field Computation by Moment Method*. New York, NY, USA: MacMillan, 1968.
[41] X. Y. Z. Xiong, L. J. Jiang, W. E. I. Sha, and Y. H. Lo, "A new EFIE method based on Coulomb gauge for the low-frequency electromagnetic analysis," *Progr. Electromagn. Res*, vol. 140, pp. 613–631, Jun. 2013.

Xiaoyan Y.Z. Xiong (S'12) received the B.S. degree from Southwest Jiaotong University, Chengdu, China, in 2008 and the M.S. degree from Peking University, Beijing, China, in 2011. She is currently working towards the Ph.D. degree at the University of Hong Kong, Hong Kong, China.

She has been with the Center of Electromagnetics and Optics, University of Hong Kong, and the Center for Computational Electromagnetics and Electromagnetics Laboratory, University of Illinois at Urbana-Champaign, since 2011 and 2014, respectively. Her research interests include computational electromagnetics, metamaterials, and nonlinear optics.

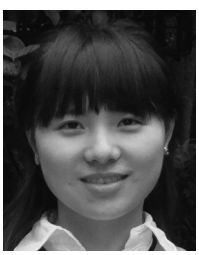

Ling Ling Meng (S'13) received the B.E. degree in information science and engineering (Honor Class) from Chien-Shiung Wu College, Southeast University, Nanjing, China, in 2011 and the M.Phil degree in electrical and electronic engineering from The University of Hong Kong, Hong Kong, China, in 2013.

Her research interests are mainly focused on applied electromagnetics, computational techniques in electrical engineering and multiphysical analysis.

Li Jun Jiang (S'01–M'04–SM'13) received the B.S. degree in electrical engineering from the Beijing University of Aeronautics and Astronautics, Beijing, China, in 1993, the M.S. degree from the Tsinghua University, Beijing, China, in 1996, and the Ph.D. degree from the University of Illinois at Urbana-Champaign, Champaign, IL, USA, in 2004.

From 1996 to 1999, he was an Application Engineer with the Hewlett-Packard Company. Since 2004, he has been a Postdoctoral Researcher, research staff member, and Senior Engineer at the IBM T.J. Watson Research Center, Yorktown Heights, NY, USA. Since the end of 2009, he is an Associate Professor with the Department of Electrical and Electronic Engineering, University of Hong Kong. His research interests focus on electromagnetics, EMC/EMI, antennas, multidisciplinary EDA solutions, RF and microwave technologies, and high performance computing (HPC), etc.

Prof. Jiang is a member of the IEEE AP-S, IEEE MTT-S, ACES, Sigma Xi, and Chinese CEM Society. In 1998, he received the HP STAR Award. In 2003, he received the IEEE MTT Graduate Fellowship Award, and in 2004 the Y.T. Lo Outstanding Research Award. In 2008, he received the IBM Research Technical Achievement Award. He was the Semiconductor Research Cooperation (SRC) Industrial Liaison for several academic projects. Since 2009, he has been the SRC Packaging High Frequency Topic TT Chair. He has served as the Technical Committee Member for IEEE EDAPS since 2010, the Scientific Committee Member of 2010 IEEE SMEE, and a Guest Associate Editor of IEEE PROCEEDINGS since 2011. He was the Scientific Consultant of HK ASTRI in 2010. He has been serving as a Reviewer of many primary professional EM related journals, and special sessions organizer and session chair of many international conferences.

Wei E.I. Sha (M'09) received the B.S. and Ph.D. degrees in electronic engineering from Anhui University, Hefei, China, in 2003 and 2008, respectively.

From July 2008 to May 2012, he was a Postdoctoral Research Fellow with the Department of Electrical and Electronic Engineering, University of Hong Kong, where he is now a Research Assistant Professor. He has coauthored two books respectively on symplectic finite-difference time-domain scheme and wavelet theory. He has authored or coauthored about 60 peer-reviewed technical Journals. He also contributed to three book chapters at Springer, CRC Press and InTech Publishers.

Dr. Sha is a member of the IEEE Antennas and Propagation Society and Photonics Society. He is also a member of OSA. He has been serving as a Reviewer for the IEEE, APS, AIP, OSA, and Nature Publishing Group journals. He also has served as a committee member of several international and local conferences. He has broad research interests in computational electromagnetics, nano-optics, solar cells, quantum optics, multiphysics, etc.

Fan Yang (S'96–M'03–SM'08) received the B.S. and M.S. degrees from Tsinghua University, Beijing, China, in 1997 and 1999, respectively, and the Ph.D. degree from the University of California at Los Angeles (UCLA), Los Angeles, CA, USA, in 2002.

From 1994 to 1999, he was a Research Assistant with the State Key Laboratory of Microwave and Digital Communications, Tsinghua University. From 1999 to 2002, he was a Graduate Student Researcher with the Antenna Laboratory, UCLA. From 2002 to 2004, he was a Postdoctoral Research Engineer and Instructor with the Electrical Engineering Department, UCLA. In 2004, he joined the Electrical Engineering Department, The University of Mississippi, University, MS, USA, as an Assistant Professor, and was promoted to an Associate Professor. In 2011, he joined the Electronic Engineering Department, Tsinghua University as a Professor, and has served as the Director of the Microwave and Antenna Institute since then. His research interests include antenna theory, designs, and measurements, electromagnetic band gap (EBG) structures and their applications, computational electromagnetics and optimization techniques, and applied electromagnetic systems. He has published over 200 journal articles and conference papers, five book chapters, and three books entitled *Scattering Analysis of Periodic Structures Using Finite-Difference Time-Domain Method* (Morgan & Claypool, 2012), *Electromagnetic Band Gap Structures in Antenna Engineering* (Cambridge Univ. Press, 2009), and *Electromagnetics and Antenna Optimization Using Taguchi's Method* (Morgan & Claypool, 2007).

Dr. Yang served as an Associate Editor of the IEEE TRANSACTIONS ON ANTENNAS AND PROPAGATION (2010–2013) and is an Associate Editor-in-Chief of *Applied Computational Electromagnetics Society* (ACES) Journal. He was the Technical Program Committee (TPC) Chair of 2014 IEEE International Symposium on Antennas and Propagation and USNC-URSI Radio Science Meeting. He has been the recipient of several prestigious awards and recognitions, including the Young Scientist Award of the 2005 URSI General Assembly and of the 2007 International Symposium on Electromagnetic Theory, the 2008 Junior Faculty Research Award of the University of Mississippi, the 2009 inaugural IEEE Donald G. Dudley Jr. Undergraduate Teaching Award, and the 2011 Recipient of Global Experts Program of China.